AGU PUBLICATIONS

Geophysical Research Letters

RESEARCH LETTER
10.1002/2017GL073754

Key Points:
- Instances of magnetic flux ropes within near-Mars magnetotail current sheets are observed that have a wide variety of orientations
- Only 3 of the 23 flux ropes analyzed here have orientations within 30 degrees of the cross-tail current direction
- Majority has large angles to the cross-tail current direction consistent with those formed in ionosphere and transported into magnetotail

Correspondence to:
T. Hara,
hara@ssl.berkeley.edu

Citation:
Hara, T., et al. (2017), On the origins of magnetic flux ropes in near-Mars magnetotail current sheets, *Geophys. Res. Lett.*, *44*, 7653–7662, doi:10.1002/2017GL073754.

Received 7 APR 2017
Accepted 16 JUL 2017
Accepted article online 24 JUL 2017
Published online 14 AUG 2017

On the origins of magnetic flux ropes in near-Mars magnetotail current sheets

Takuya Hara[1], Yuki Harada[1,2], David L. Mitchell[1], Gina A. DiBraccio[3], Jared R. Espley[3], David A. Brain[4], Jasper S. Halekas[2], Kanako Seki[5], Janet G. Luhmann[1], James P. McFadden[1], Christian Mazelle[6], and Bruce M. Jakosky[4]

[1]Space Sciences Laboratory, University of California, Berkeley, California, USA, [2]Department of Physics and Astronomy, University of Iowa, Iowa City, Iowa, USA, [3]NASA Goddard Space Flight Center, Greenbelt, Maryland, USA, [4]Laboratory for Atmospheric and Space Physics, University of Colorado Boulder, Boulder, Colorado, USA, [5]Department of Earth and Planetary Science, Graduate School of Science, University of Tokyo, Tokyo, Japan, [6]IRAP, University of Toulouse, CNRS, UPS, CNES, Toulouse, France

Abstract We analyze Mars Atmosphere and Volatile EvolutioN (MAVEN) observations of magnetic flux ropes embedded in Martian magnetotail current sheets, in order to evaluate the role of magnetotail reconnection in their generations. We conduct a minimum variance analysis to infer the generation processes of magnetotail flux ropes from the geometrical configuration of the individual flux rope axial orientation with respect to the overall current sheet. Of 23 flux ropes detected in current sheets in the near-Mars (~1–3 Martian radii downstream) magnetotail, only 3 (possibly 4) can be explained by the magnetotail reconnection scenario, while the vast majority of the events (19 events) are more consistent with flux ropes that are originally generated in the dayside ionosphere and subsequently transported into the nightside magnetotail. The mixed origins of the detected flux ropes imply complex nature of generation and transport of Martian magnetotail flux ropes.

1. Introduction

Mars lacks a global intrinsic magnetic field; therefore, the interplanetary magnetic field (IMF) embedded in the solar wind plays a significant role in the formation of the Martian induced magnetosphere by draping around the planet. The localized crustal magnetic fields are nonuniformly distributed over the Martian surface [e.g., *Acuña et al.*, 1998, 1999], resulting in a complex electromagnetic field configuration in the Martian plasma environment. As the Martian upper atmosphere can be energized via its direct interaction with the solar wind, the Martian magnetotail is one of the most important plasma regimes in which a large amount of the Martian ionospheric plasma is accelerated, leading to atmospheric escape into the interplanetary space [e.g., *Lundin et al.*, 1989; *Barabash et al.*, 2007; *Dong et al.*, 2015]. A wealth of in situ spacecraft plasma and field measurements over a few decades has been unraveling various plasma dynamics operating in the magnetotail of unmagnetized planets, such as Mars and Venus, including the ion acceleration mechanisms through the central plasma sheet [e.g., *Dubinin et al.*, 1993, 2013; *Fedorov et al.*, 2006, 2008], complex magnetic topologies [e.g., *Brain et al.*, 2007; *Chai et al.*, 2016; *Xu et al.*, 2017], tail flapping motions [e.g., *Rong et al.*, 2015; *DiBraccio et al.*, 2017], planetward ion flows [e.g., *Dubinin et al.*, 2012; *Harada et al.*, 2015a; *Kollmann et al.*, 2016] presumably associated with magnetic reconnection [e.g., *Zhang et al.*, 2012; *Harada et al.*, 2015b, 2017], and magnetic flux ropes [e.g., *Eastwood et al.*, 2012; *DiBraccio et al.*, 2015a].

Flux ropes are characteristic twisted helical magnetic field structures detected throughout the solar system [e.g., *Russell and Elphic*, 1979]. In particular, detached flux ropes (as well as plasma clouds) filled with a large amount of ionospheric plasmas can potentially provide a significant contribution to the ion escape from Mars [e.g., *Brain et al.*, 2010; *Halekas et al.*, 2016]. Indeed, these helical flux rope structures are quite common in the Martian plasma environment [e.g., *Cloutier et al.*, 1999; *Vignes et al.*, 2004; *Brain et al.*, 2010; *Briggs et al.*, 2011; *Hara et al.*, 2014a, 2014b]. Some researchers proposed that the ionospheric flux ropes are formed by magnetic reconnection between crustal magnetic field themselves [*Brain et al.*, 2010; *Beharrell and Wild*, 2012] or between the crustal field and the overlaid IMF [*Hara et al.*, 2014b, 2017]; however, the physical mechanisms responsible for generating flux ropes in the Martian induced magnetotail remain poorly understood.

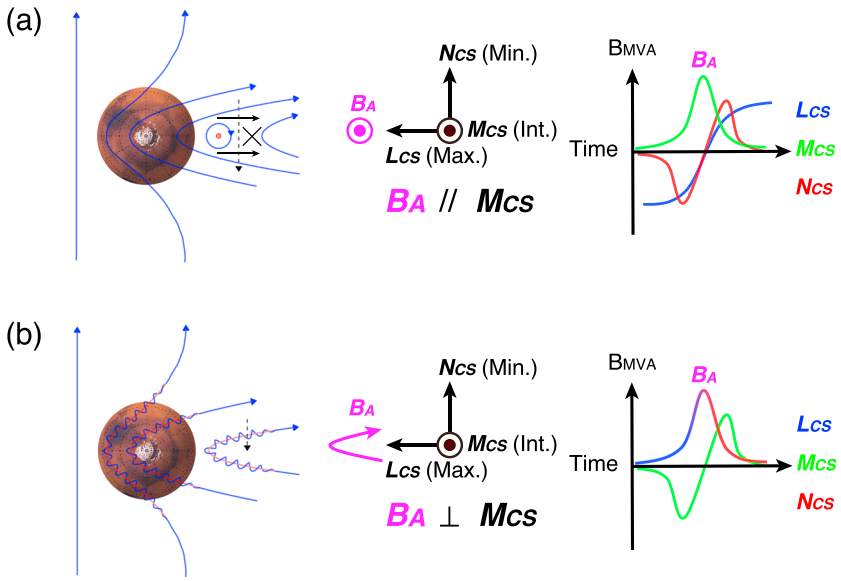

Figure 1. Schematic illustrations of a flux rope embedded in the Martian magnetotail current sheet (left) and the anticipated magnetic field variations of the tail flux rope (right), viewed from the current sheet based minimum variance analysis (CS-B_{MVA}) coordinates. A flux rope is assumed to be formed (a) by magnetotail reconnection and (b) in the dayside and is subsequently transported to the nightside magnetotail region. Blue arrows are magnetic field lines draped around the planet. Magenta lines and arrows are the anticipated flux rope axial orientation ($\boldsymbol{B}_A$). The spacecraft motion is described as the dashed black arrows.

Here we investigate the generation mechanisms of flux ropes, specifically focusing on those embedded in Martian magnetotail current sheets, based on the Mars Atmosphere and Volatile EvolutioN (MAVEN) comprehensive plasma and field measurements [e.g., *Jakosky et al.*, 2015]. In this paper, we address the issue on the relative role of magnetotail reconnection in the formation of flux ropes observed in Martian magnetotail current sheets. We test two possible scenarios for the flux rope formation.

First, magnetic reconnection within magnetotail current sheets provides a straightforward explanation for the generation of Martian magnetotail flux ropes (Figure 1a), analogous to the terrestrial magnetotail plasmoid formation [e.g., *Eastwood and Kiehas*, 2015, and references therein]. Indeed, several studies have demonstrated the presence of magnetic reconnection signatures in the Martian plasma environment [e.g., *Eastwood et al.*, 2008; *Halekas et al.*, 2009; *Harada et al.*, 2015b, 2017]. *Eastwood et al.* [2012] presented Mars Global Surveyor (MGS) observations of a chain of flux ropes in the Martian magnetotail current sheet. Based on the magnetic field geometrical configurations of the individual flux ropes with respect to the overall current sheet derived from the minimum variance analysis (MVA) [e.g., *Sonnerup and Scheible*, 1998], they interpreted that these multiple flux ropes can be generated by magnetic reconnection subsequently rather than simultaneously. They also pointed out the potential importance of the crustal fields leading to thin current sheet formation, because the observed current sheet was rather thick unfavorable to magnetotail reconnection, and a significant crustal field region was located on the dayside terminator upstream from the observed chain of flux ropes [*Eastwood et al.*, 2012]. *DiBraccio et al.* [2015a] also reported a magnetotail flux rope signature from the MAVEN magnetic field measurements.

Alternatively, we can explore the second possibility that does not necessitate magnetotail reconnection: transport of flux ropes that are originally generated in the dayside ionosphere through plasma instabilities such as helical kink, Kelvin-Helmholtz instabilities [e.g., *Elphic and Russell*, 1983; *Wolff et al.*, 1980; *Ruhunusiri et al.*, 2016], and magnetic reconnection in consequence of interactions between the IMF and crustal fields [e.g., *Hara et al.*, 2014b, 2017], or dayside magnetic reconnection analogous to the terrestrial flux transfer events [see, e.g., *Hasegawa*, 2012, and references therein]. As illustrated in Figure 1b, these helical draped magnetic field lines can be subsequently transported into the nightside magnetotail forming the current sheet, allowing spacecraft to detect them as flux ropes embedded in the magnetotail current sheets. Indeed, *Slavin et al.* [2009] have proposed this scenario and actually found the event in near-Venus magnetotail.

The detailed explanations for generation processes of flux ropes in the dayside ionospheres of unmagnetized planets are extensively given by *Luhmann and Cravens* [1991].

In a similar manner to *Eastwood et al.* [2012], we perform a minimum variance analysis (MVA) [e.g., *Sonnerup and Scheible*, 1998] on the MAVEN magnetic field data to define two different coordinates: (i) one relevant to the overall current sheet configuration (CS-B_{MVA}) and (ii) the other representing the local structure of individual flux ropes (FR-B_{MVA}). Figure 1 summarizes geometrical configurations of the magnetotail current sheet and flux rope, and the anticipated magnetic field variations during the flux rope encounter in the overall current sheet coordinates (CS-B_{MVA}). For a flux rope formed by magnetic reconnection in the magnetotail current sheet (Figure 1a), the flux rope axial core field ($\boldsymbol{B}_A$) is expected to be oriented parallel to the current sheet intermediate variance ($\boldsymbol{M}_{CS}$) direction (the cross-tail current direction). Hence, in the time series of magnetic fields in the CS-B_{MVA} coordinates, a peak magnetic field should be observed in the $\boldsymbol{M}_{CS}$ direction. Meanwhile, a magnetic field component of the current sheet maximum variance ($\boldsymbol{L}_{CS}$) direction changes its sign during the flux rope encounter. In addition, a bipolar signature will be found in the current sheet minimum variance ($\boldsymbol{N}_{CS}$) direction if the flux rope is moving tailward with a speed sufficiently faster than the spacecraft velocity across the spacecraft as suggested by *Eastwood et al.* [2012]. We note that the alignment of the flux rope axial core field with the overall current sheet $\boldsymbol{M}_{CS}$ direction is expected for the flux rope formation via magnetotail reconnection irrespective of the origins of current sheets (i.e., between draped IMFs, crustal fields, or both).

The expected magnetic field configuration is totally different for a flux rope that is originally formed in the dayside ionosphere and subsequently transported into the nightside magnetotail (Figure 1b). In this case, the flux rope axial core field ($\boldsymbol{B}_A$) should be oriented perpendicular to the current sheet intermediate variance ($\boldsymbol{M}_{CS}$) direction. Meanwhile, a bipolar signature should be found in the current sheet ($\boldsymbol{M}_{CS}$) direction across the flux rope. Since the flux rope core field ($\boldsymbol{B}_A$) is oriented on the $\boldsymbol{L}_{CS}$-$\boldsymbol{N}_{CS}$ plane in the CS-B_{MVA} coordinates, a peak field should be found in either $\boldsymbol{L}_{CS}$ or $\boldsymbol{N}_{CS}$ directions depending on the crossing geometry of the spacecraft and individual flux ropes.

2. Flux Rope Events

This section presents two events to demonstrate the methodology of inferring the generation processes of magnetotail flux ropes from the geometrical configurations of the individual flux rope axial orientation with respect to the overall current sheet.

2.1. Magnetotail Reconnection Event

Figure 2 presents an example of the MAVEN plasma and magnetic field observations across a single current sheet in the Martian magnetotail on 4 December 2014 (orbit #354). Figure 2f shows the vector magnetic field measured by the MAG instrument [*Connerney et al.*, 2015] in the Mars-centered Solar Orbital (MSO) coordinates. The MSO coordinates are defined with X_{MSO} axis toward the Sun, the Z_{MSO} axis perpendicular to the ecliptic pointing to the northern hemisphere, and Y_{MSO} axis completing the right-hand system. Figure 2f clearly shows that the B_X component (blue) reversed its sign from negative to positive, indicating that MAVEN crossed the magnetotail current sheet. Meanwhile, as highlighted by the gray horizontal bar in Figure 2e, the local magnetic field enhancement, with a peak strength ~12 nT, was embedded in the overall magnetotail current sheet structure.

Figures 2h–2j represent the result of MVA (FR-B_{MVA}), which is performed to the MAG data during the gray horizontal bar. Figure 2h shows that the flux rope maximum variance ($\boldsymbol{L}_{FR}$) direction changes its sign, and the unimodal peak is found in the flux rope intermediate variance ($\boldsymbol{M}_{FR}$) direction. The hodogram in Figure 2i also shows a smooth circular rotation pattern, which is a characteristic signature of a flux rope [e.g., *Vignes et al.*, 2004]. Therefore, we adopt the $\boldsymbol{M}_{FR}$ axis as the flux rope axial core direction to be $\boldsymbol{B}_A = [0.347, -0.292, -0.891]$ in the MSO coordinates.

In order to determine the overall current sheet geometry (CS-B_{MVA}), Figure 2f is transformed into Figure 2g by performing the MVA to the time segment between vertical magenta dashed lines in Figure 2. The CS-B_{MVA} coordinates are thus found to be $\boldsymbol{L}_{CS} = [0.849, 0.108, 0.517]$, $\boldsymbol{M}_{CS} = [0.511, -0.416, -0.752]$, and $\boldsymbol{N}_{CS} = [0.134, 0.903, -0.409]$ in the MSO coordinates, respectively. The angle between the $\boldsymbol{B}_A$ and $\boldsymbol{M}_{CS}$ axis turns out to be ~14°, i.e., the flux rope axial core field ($\boldsymbol{B}_A$) is approximately parallel to the current sheet intermediate variance ($\boldsymbol{M}_{CS}$) direction. Besides, the small bipolar signature is found in the $\boldsymbol{N}_{CS}$ component in Figure 2g. These signatures are in good agreement with the geometrical configuration in Figure 1a. We can thus conclude

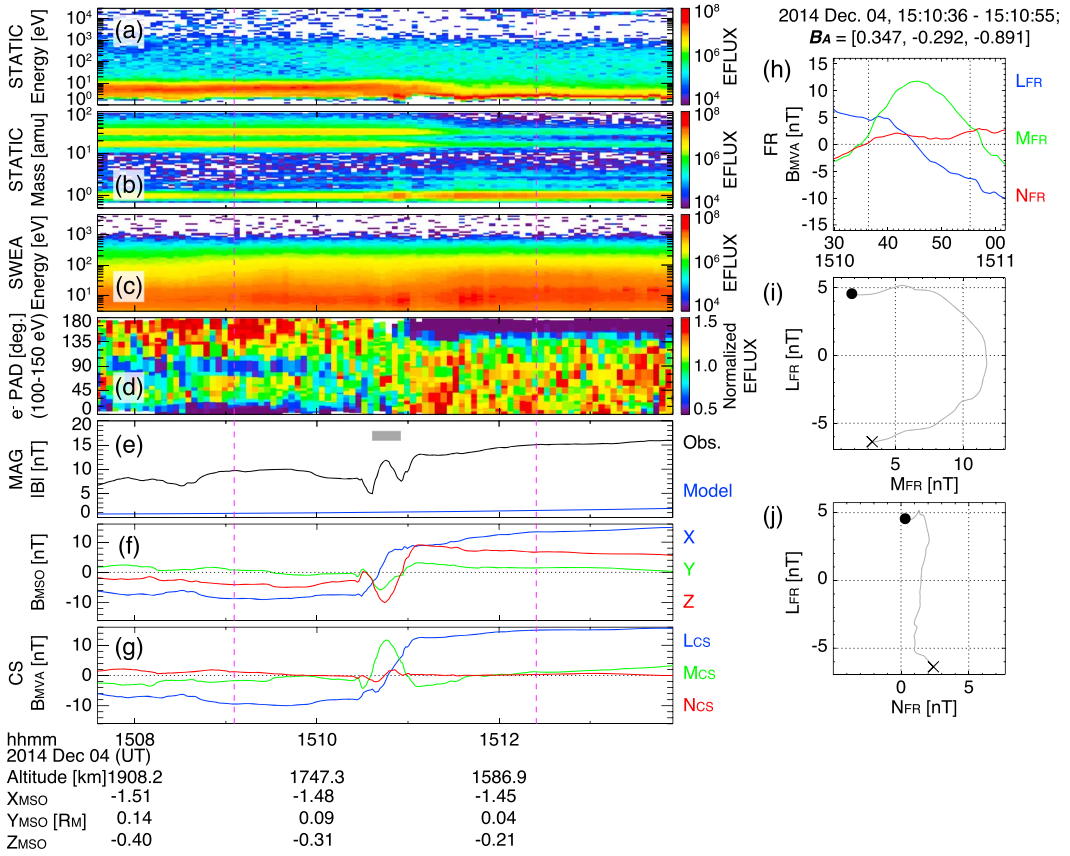

Figure 2. Overview of the MAVEN flux rope observations in the Martian magnetotail current sheet on 4 December 2014 (Orbit #354): STATIC measurements of ions (a) omnidirectional energy and (b) mass spectra shown in units of differential energy flux (EFLUX) of eV/cm^2/str/s/eV. SWEA measurements of electrons (c) omnidirectional energy spectra shown also in units of differential energy flux and (d) the normalized pitch angle distributions with energies between 100 and 150 eV. MAG measurements of magnetic field (e) amplitude (black) together with the modeled crustal field (blue) [*Morschhauser et al.*, 2014] and vector components in (f) the MSO coordinates and transformed into the (g) current sheet-based minimum variance analysis (CS-B_{MVA}) coordinates. A minimum variance analysis is performed by the time interval between two magenta vertical dashed lines in order to determine the CS-B_{MVA} coordinates. A magnetotail flux rope measurement is highlighted by the gray horizontal bar in Figure 2e. (h) Time profile and (i, j) hodograms of the vector magnetic field components transformed into the flux rope-based minimum variance analysis (FR-B_{MVA}) coordinates. Black filled circles (crosses) in Figures 2i and 2j are start (end) points.

that the observed properties in this event are consistent with a flux rope generated by reconnection in the magnetotail current sheet.

Figures 2a–2d provide the context of local plasmas during this event. Throughout the current sheet crossings, the SupraThermal and Thermal Ion Composition (STATIC) ion instrument on board MAVEN [*McFadden et al.*, 2015] observed multiple ion species including H^+, O^+, and O_2^+ (Figures 2a and 2b). The Solar Wind Electron Analyzer (SWEA) electron measurements [*Mitchell et al.*, 2016] in Figures 2c and 2d indicate that one-sided loss cone distributions were detected just before and after the current sheet crossing. It implies draped or open magnetic topologies around the event, i.e., at least one-sided ends connected to the solar wind [see, e.g., *Brain et al.*, 2007; *Xu et al.*, 2017].

2.2. Dayside Structure Transport Event

Figure 3 presents another current sheet crossing on 19 September 2015 (orbit #1895); however, this event has a couple of remarkable characteristics different from Figure 2. In terms of the magnetic field measurements in Figures 3e and 3f, MAVEN consecutively detected four distinct magnetic field enhancements during the magnetotail current sheet crossing inferred from the B_X reversal. We can confirm from the MVA results in Figures 3h–3k that all the magnetic field enhancements are owing to the flux rope encounters. Since the bipolar-like signatures are found in the $\boldsymbol{L}_{FR}$ direction, and the unimodal peaks are found in the $\boldsymbol{M}_{FR}$ direction,

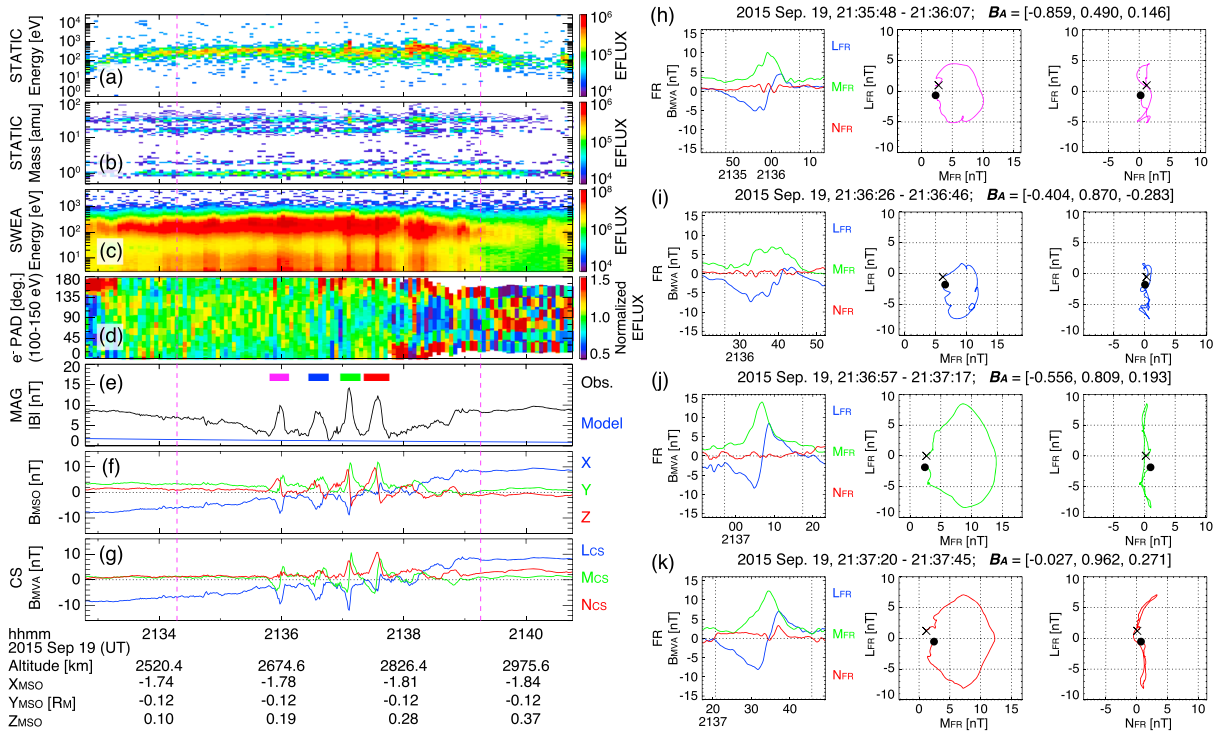

Figure 3. Overview of the MAVEN flux rope observations in the Martian magnetotail current sheet on 19 September 2015 (Orbit #1895): (a–g) The same as Figures 2a–2g; however, four flux ropes are consecutively observed in the Martian magnetotail current sheet, which are highlighted by horizontal magenta, blue, green, and red bars in Figure 3e. (h–k) Time profiles and hodograms of individual tail flux ropes transformed into the FR-B_{MVA} coordinates. Their formats are mostly identical to Figures 2h–2j.

the individual flux rope intermediate variance ($\boldsymbol{M}_{FR}$) axes can be estimated as the axial core directions for each flux rope to be $\boldsymbol{B}_A = [-0.859, 0.490, 0.146]$ (magenta; Figure 3h), $[-0.404, 0.870, -0.283]$ (blue; Figure 3i), $[-0.566, 0.809, 0.193]$ (green; Figure 3j), and $[-0.027, 0.962, 0.271]$ (red; Figure 3k). Interestingly, the estimated flux rope axis gradually varies from the $-X_{MSO}$ to $+Y_{MSO}$ directions.

We now compare the multiple flux rope measurements presented here to the MGS measurement of a chain of flux ropes in the Martian magnetotail current sheet reported by *Eastwood et al.* [2012]. They concluded that a chain of flux ropes were generated by subsequent magnetotail reconnection, because the estimated flux rope axial orientations ($\boldsymbol{B}_A$) tend to be approximately parallel to the current sheet intermediate variance ($\boldsymbol{M}_{CS}$) direction, and the flux rope bipolar signatures are seen in the $\boldsymbol{N}_{CS}$ direction in the CS-B_{MVA} coordinates as shown in Figure 1a [*Eastwood et al.*, 2012]. Unlike *Eastwood et al.*'s [2012] measurements, the flux rope axial orientations of this event exhibit large angles with respect to the overall current sheet $\boldsymbol{M}_{CS}$ direction; the CS-B_{MVA} coordinates for this event are found to be $\boldsymbol{L}_{CS} = [0.942, -0.256, -0.215]$, $\boldsymbol{M}_{CS} = [-0.031, 0.574, -0.818]$, and $\boldsymbol{N}_{CS} = [0.333, 0.778, -0.533]$ in the MSO coordinates. Therefore, the angles of $\boldsymbol{B}_A$ relative to the $\boldsymbol{M}_{CS}$ axis turn out to be ~79 (magenta; Figure 3h), ~42 (blue; Figure 3i), ~71 (green; Figure 3j), and ~71° (red; Figure 3k), i.e., most of the flux rope axial core fields ($\boldsymbol{B}_A$) are nearly perpendicular to the current sheet intermediate variance ($\boldsymbol{M}_{CS}$) direction. This configuration cannot be explained by the magnetotail reconnection scenario, in which $\boldsymbol{B}_A$ should be aligned with $\boldsymbol{M}_{CS}$ (Figure 1a). Figure 3g clearly shows that the bipolar signature during every flux rope encounter is found in the current sheet intermediate variance ($\boldsymbol{M}_{CS}$) direction; therefore, these flux rope magnetic field variations in the CS-B_{MVA} coordinates are in good agreement with Figure 1b, suggesting that these flux ropes are consistent with those generated in the dayside ionosphere and transported into the magnetotail.

In terms of plasma signatures (Figures 3a–3d), MAVEN observed typical energetic plasmas with energies up to a few hundreds of eV, which are accelerated in the Martian magnetotail current sheet [e.g., *Dubinin et al.*, 1993; *Dubinin and Fraenz*, 2015, and references therein]. STATIC simultaneously recorded multiple ion species including H^+, O^+, and O_2^+ across the current sheet, similar to Figure 2. Interestingly, planetary heavy ions are likely accelerated up to almost the same energy regardless of their species. It can be interpreted that the

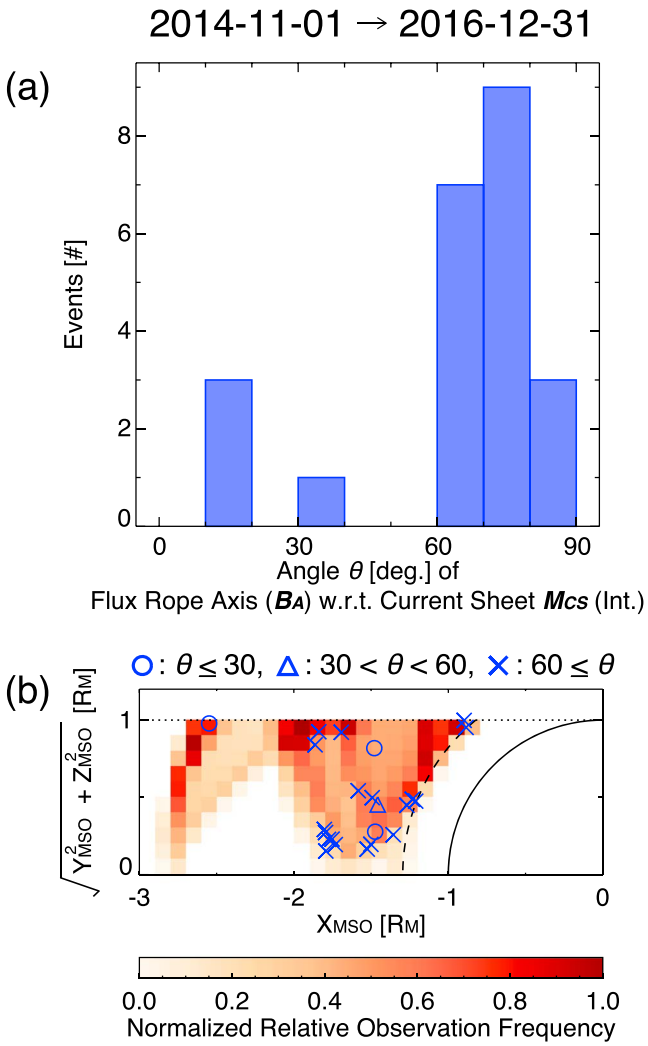

Figure 4. (a) Histogram of the Martian flux ropes observed in the magnetotail current sheet as a function of the angle of the flux rope axis ($\boldsymbol{B}_A$) with respect to the current sheet intermediate variance ($\boldsymbol{M}_{CS}$) direction. (b) Events distributions onto cylindrical $X - \sqrt{Y^2 + Z^2}$ coordinates in the MSO coordinates. The background contour is the relative MAVEN observations frequency in the magnetotail, which is normalized by the highest bin. Black dashed curve is the lowest altitude of 1000 km, from which we surveyed magnetotail flux ropes.

planetary heavy ions are accelerated by the Hall electric field driven by differential motion between unmagnetized ions and magnetized electrons accelerated tailward by $\boldsymbol{j} \times \boldsymbol{B}$ force [e.g., *Dubinin et al.*, 1993; *Dubinin and Fraenz*, 2015].

3. Statistical Results

In this section, we statistically survey flux ropes embedded in the magnetotail current sheet from November 2014 (Orbit #178) to December 2016 (Orbit #4383). We only use the data obtained when MAVEN was located in the geometric shadow at altitudes higher than 1000 km, thereby focusing on the high-altitude region of the Martian magnetotail and eliminating direct influence of complex crustal magnetic fields at low altitudes on the flux rope detection algorithm as described below: First, we automatically searched for a local peak of noncrustal magnetic field strengths (obtained by subtracting the model crustal field [*Morschhauser et al.*, 2014] from the observed field). Then the MVA was performed for the time intervals between the nearest magnetic dips adjacent to the local magnetic peak. Based on these local MVA results (FR-B_{MVA}), we identified possible flux rope events by applying the following selection criteria: (1) the local magnetic peak is stronger than each of the nearest magnetic dips by at least 3 nT, (2) the bipolar and unimodal magnetic field signatures must be found in either the maximum or intermediate variance directions of the FR-B_{MVA} coordinates, and (3) each of the bipolar peak amplitudes is greater than 2 nT. We counted each individual flux rope in case multiple flux ropes are seen in the single magnetotail current crossing like Figure 3. In this way, we tentatively found 169 candidate flux rope events from 1962 unique orbits in total. Of the 169 candidate events, we selected 27 events with stable, single magnetotail current sheet crossings to ensure well-defined configurations of the overall current sheets (CS-B_{MVA}). A basic idea to examine stable, single current sheet crossings is similar to the previous studies [*Halekas and Brain*, 2010; *Harada et al.*, 2017]. After removing 4 improper events whose hodograms did not show simple circular patterns, the remaining 23 flux rope events were finally utilized for our statistical study. We note that the Figure 3i (blue) event does not satisfy the selection criterion (3), and it was excluded from the statistical results.

Figure 4a shows the histogram of the identified 23 magnetotail flux rope events as a function of the angle ($\equiv \theta$) of the flux rope axial orientation ($\boldsymbol{B}_A$) with respect to the current sheet intermediate variance ($\boldsymbol{M}_{CS}$) axis. We took the polarity uncertainty of the current sheet intermediate variance ($\boldsymbol{M}_{CS}$) axis into account, and the angle in Figure 4 ranges between 0 and 90° rather than between 0 and 180°. As shown in Figure 1, if the identified flux ropes are generated by magnetotail reconnection, the flux rope axial core ($\boldsymbol{B}_A$) direction is expected

to be oriented parallel to the current sheet intermediate variance ($\boldsymbol{M}_{CS}$) axis, i.e., $\theta \sim 0°$. On the other hand, if they are generated in the dayside ionosphere and then transported into the magnetotail, the flux rope axial core ($\boldsymbol{B}_{A}$) direction will be oriented perpendicular to the current sheet intermediate variance ($\boldsymbol{M}_{CS}$) axis, i.e., $\theta \sim 90°$. In Figure 4a, we observe 19 events that can be categorized into the dayside structure transport scenario ($\theta \geq 60°$), and only 3 events that are consistent with magnetotail reconnection ($\theta \leq 30°$). Therefore, our statistical result suggests that magnetotail flux ropes consistent with the dayside structure transport scenario are more frequently observed by MAVEN than those generated by magnetotail reconnection.

Figure 4b indicates that these events are largely detected in the central plasma sheet while the spatial data coverage lacked at ~2 Martian radii and farther downstream from Mars. Although the events are found in both northern and southern hemispheres, interestingly, they tend to be detected more frequently in the southern hemisphere rather than in the northern hemisphere (not shown here), indicating that the crustal magnetic field could play some roles in generating flux ropes embedded in the magnetotail current sheets. These 23 magnetotail flux rope events possess some similar features regardless of their generation processes. For example, their observed duration is about several tens of seconds with a peak field ranging between ~10 and 25 nT. Multiple ion species including H^+, O^+, and O_2^+ are simultaneously recorded during their encounters that is consistent with the previous MAVEN observations [*Hara et al.*, 2015, 2016, 2017]. However, it should be noted that the flux ropes with $\theta \geq 60°$ tend to be observed in a series of multiple flux rope signatures across a single magnetotail current sheet as shown in Figure 3.

4. Discussion and Conclusions

In this paper, we investigated the Martian flux ropes observed by MAVEN in magnetotail current sheets in order to constrain their generation mechanisms. Comparing the geometrical configurations between the current sheet and flux rope based on the minimum variance analysis (MVA), we categorized the magnetotail flux ropes into two different types as shown in Figure 1: one consistent the flux ropes formed by magnetotail reconnection and the other consistent with flux ropes generated in the dayside ionosphere and transported into the nightside magnetotail region. Statistical survey shows that MAVEN detected both types, but the latter was much more frequently detected than the former.

One important question associated with our results is why MAVEN did not frequently observe flux ropes generated by magnetotail reconnection. MAVEN has detected magnetic reconnection signatures within the central tail current sheet in the near-Mars magnetotail at ~1.3 Martian radii presented by *Harada et al.* [2015b]. They further reveal that the in situ reconnection signatures, characterized by Hall magnetic fields, are commonly observed in about 1–2 Martian radii downstream from Mars [*Harada et al.*, 2017]. On one hand, the recent MHD coupling to the particle-in-cell simulation predicts that flux ropes which are generated by magnetotail reconnection fully develop typically at ~2 Martian radii and farther downstream from Mars, and this region has been poorly explored by MAVEN (see Figure 4b). This possibility could explain why the magnetotail reconnection flux ropes are so rare in the current MAVEN data set.

Another concern associated with the dayside structure transport model is how long flux ropes generated in the dayside ionosphere can retain their structures on the way to the nightside magnetotail. Several previous numerical simulations predicted that flux ropes generated in the Venus dayside ionosphere are maintained for ~10 min to several hours [*Luhmann et al.*, 1984; *Shinagawa and Cravens*, 1988; *Shimazu and Tanaka*, 2008], which could provide sufficient time for transport of flux ropes out of the ionosphere into the magnetotail region. Previous two spacecraft measurements also confirmed that it took ~10 min for the IMF to drape around the Venus dayside ionosphere and to transport into the nightside magnetotail [e.g., *Huddleston et al.*, 1996; *Slavin et al.*, 2009]. This time scale might be too short for the draped IMF to form the thin magnetotail current sheet.

It should be noted that flux ropes generated by magnetotail reconnection (blue circles in Figure 4b) tend to be found only in the southern hemisphere (not shown here). As pointed out by *Eastwood et al.* [2012], it might indicate that crustal magnetic fields would play some roles to drive the plasma convection enhancement in the Martian induced magnetosphere, allowing magnetotail current sheets to be thin, favorably leading to magnetic reconnection.

There are mainly two caveats associated with the MVA for this study: One is the uncertainty in determining the CS-B_{MVA} coordinates to compare the geometrical configuration of the individual flux rope axial orientation

with respect to the overall current sheet. Since the structures of the magnetotail flux ropes are embedded in the current sheets, eigenvalues ratio of the intermediate variance direction ($\boldsymbol{M}_{CS}$) to the minimum variance direction ($\boldsymbol{N}_{CS}$) might be close to ~1 for some cases. However, the orientation of the maximum variance direction ($\boldsymbol{L}_{CS}$) will be precisely determined because of the current sheet crossings. Therefore, we will be able to at least identify the dayside structure transport events (Figure 1b), because it is likely that a peak signature can be seen in the $\boldsymbol{L}_{CS}$ direction during the flux rope encounters, even though the MVA cannot precisely determine the $\boldsymbol{M}_{CS}$ and $\boldsymbol{N}_{CS}$ directions. Indeed, we observed at least eight $\boldsymbol{L}_{CS}$ dominant events with an angle of the flux rope axis with respect to the $\boldsymbol{L}_{CS}$ direction smaller than 30°, suggesting that the dayside structure transport scenario (Figure 1b) for which magnetotail reconnection is not necessary turns out to be one of the significant mechanisms in generating flux ropes within near-Mars magnetotail current sheets.

The other is that some previous studies pointed out that the MVA results might be unreliable in determining the flux rope axial orientation in some cases, depending on the crossing geometry of the spacecraft relative to the flux rope structure [e.g., *Xiao et al.*, 2004; *Rong et al.*, 2013]. However, in this study, we have visually inspected each individual flux rope events to confirm that their axial orientations (core field directions) adopted from the MVA results have the unimodal peak signature. As mentioned in section 3, our automated method to identify candidate flux rope events requires that the bipolar and unimodal magnetic field signatures must be found in either the maximum or intermediate variance directions of the FR-B_{MVA} coordinates. Therefore, our method automatically disregards cases with fluctuations that are not indicative flux rope signatures, e.g., both directions have bipolar or unimodal signatures. In order to examine the potential influence of the crossing geometry on the determination of the flux rope axial orientation, we have implemented a force-free flux rope fitting model (see, e.g., *Lepping et al.* [1990] and *DiBraccio et al.* [2015b] in detail) and computed the impact parameter, i.e., the closest distance between the spacecraft trajectory and the central axis of the flux rope. The estimated mean impact parameter with a standard deviation (normalized by the estimated flux rope radius) is 0.19 ± 0.16, indicating that MAVEN traveled relatively close to the centers of the flux ropes. In such cases, the unimodal peak in the FR-B_{MVA} coordinates corresponds to the flux rope core field ($\boldsymbol{B}_A$). Therefore, we are confident in our approach of adopting the unimodal peak found in FR-B_{MVA} coordinates as the flux rope axial orientation.

The statistical results exhibit the mixture of different types of magnetotail flux ropes, implying complex nature of their origins. Neither one of the proposed formation scenarios can explain all of the detected flux ropes. The possible sampling bias discussed above further complicates the interpretation. Care must be taken when discussing consequences of the observed magnetotail flux ropes (e.g., ion escape related to detached flux ropes) because different generation mechanisms of flux ropes are likely to play differently roles in the dynamics of the ionosphere and magnetosphere of Mars.

Acknowledgments
The authors wish to acknowledge valuable supports from the science team members of the MAVEN mission. This study presented in this paper was funded by the NASA MAVEN project. Analysis of SWEA data was partially supported by CNES. K.S. was supported by Grant-in-Aid for Scientific Research (A) 16H02229 and (B) 15H0731 of Japan Society for the Promotion of Science (JSPS). The MAVEN data used in this paper are publicly available in NASA's Planetary Data System (https://pds-ppi.igpp.ucla.edu).

References

Acuña, M. H., et al. (1998), Magnetic field and plasma observations at Mars: Initial results of the Mars Global Surveyor mission, *Science*, *279*, 1676–1680, doi:10.1126/science.279.5357.1676.

Acuña, M. H., et al. (1999), Global distribution of crustal magnetization discovered by the Mars Global Surveyor MAG/ER experiment, *Science*, *284*, 790–793, doi:10.1126/science.284.5415.790.

Barabash, S., A. Fedorov, R. Lundin, and J.-A. Sauvaud (2007), Martian atmospheric erosion rates, *Science*, *315*, 501–503, doi:10.1126/science.1134358.

Beharrell, M. J., and J. A. Wild (2012), Stationary flux ropes at the southern terminator of Mars, *J. Geophys. Res.*, *117*, A12212, doi:10.1029/2012JA017738.

Brain, D. A., R. J. Lillis, D. L. Mitchell, J. S. Halekas, and R. P. Lin (2007), Electron pitch angle distributions as indicators of magnetic field topology near Mars, *J. Geophys. Res.*, *112*, A09201, doi:10.1029/2007JA012435.

Brain, D. A., A. H. Baker, J. Briggs, J. P. Eastwood, J. S. Halekas, and T.-D. Phan (2010), Episodic detachment of Martian crustal magnetic fields leading to bulk atmospheric plasma escape, *Geophys. Res. Lett.*, *37*, L14108, doi:10.1029/2010GL043916.

Briggs, J. A., D. A. Brain, M. L. Cartwright, J. P. Eastwood, and J. S. Halekas (2011), A statistical study of flux ropes in the Martian magnetosphere, *Planet. Space Sci.*, *59*, 1498–1505, doi:10.1016/j.pss.2011.06.010.

Chai, L., et al. (2016), An induced global magnetic field looping around the magnetotail of Venus, *J. Geophys. Res. Space Physics*, *121*, 688–698, doi:10.1002/2015JA021904.

Cloutier, P. A., et al. (1999), Venus-like interaction of the solar wind with Mars, *Geophys. Res. Lett.*, *26*, 2685–2688, doi:10.1029/1999GL900591.

Connerney, J. E. P., J. Espley, P. Lawton, S. Murphy, J. Odom, R. Oliversen, and D. Sheppard (2015), The MAVEN magnetic field investigation, *Space Sci. Rev.*, *195*, 257–291, doi:10.1007/s11214-015-0169-4.

DiBraccio, G. A., et al. (2015a), Magnetotail dynamics at Mars: Initial MAVEN observations, *Geophys. Res. Lett.*, *42*, 8828–8837, doi:10.1002/2015GL065248.

DiBraccio, G. A., et al. (2015b), MESSENGER observations of flux ropes in Mercury's magnetotail, *Planet. Space Sci.*, *115*, 77–89, doi:10.1016/j.pss.2014.12.016.

DiBraccio, G. A., et al. (2017), MAVEN observations of tail current sheet flapping at Mars, *J. Geophys. Res. Space Physics*, *122*, 4308–4324, doi:10.1002/2016JA023488.
Dong, Y., X. Fang, D. A. Brain, J. P. McFadden, J. S. Halekas, J. E. Connerney, S. M. Curry, Y. Harada, J. G. Luhmann, and B. M. Jakosky (2015), Strong plume fluxes at Mars observed by MAVEN: An important planetary ion escape channel, *Geophys. Res. Lett.*, *42*, 8942–8950, doi:10.1002/2015GL065346.
Dubinin, E., and M. Fraenz (2015), Magnetotails of Mars and Venus, in *Magnetotails in the Solar System, Geophys. Monogr. Ser.*, vol. 207, edited by A. Keiling, C. M. Jackman, and P. A. Delamere, pp. 34–59, John Wiley, Hoboken, N. J., doi:10.1002/9781118842324.ch3.
Dubinin, E., R. Lundin, O. Norberg, and N. Pissarenko (1993), Ion acceleration in the Martian tail: Phobos observations, *J. Geophys. Res.*, *98*, 3991–3997, doi:10.1029/92JA02233.
Dubinin, E., M. Fraenz, J. Woch, T. L. Zhang, J. Wei, A. Fedorov, S. Barabash, and R. Lundin (2012), Bursty escape fluxes in plasma sheets of Mars and Venus, *Geophys. Res. Lett.*, *39*, L01104, doi:10.1029/2011GL049883.
Dubinin, E., M. Fraenz, T. L. Zhang, J. Woch, Y. Wei, A. Fedorov, S. Barabash, and R. Lundin (2013), Plasma in the near Venus tail: Venus Express observations, *J. Geophys. Res. Space Physics*, *118*, 7624–7634, doi:10.1002/2013JA019164.
Eastwood, J. P., and S. A. Kiehas (2015), Origin and evolution of plasmoids and flux ropes in the magnetotails of Earth and Mars, in *Magnetotails in the Solar System, Geophys. Monogr. Ser.*, vol. 207, edited by A. Keiling, C. M. Jackman, and P. A. Delamere, pp. 269–287, John Wiley, Hoboken, N. J., doi:10.1002/9781118842324.ch16.
Eastwood, J. P., D. A. Brain, J. S. Halekas, J. F. Drake, T. D. Phan, M. Øieroset, D. L. Mitchell, R. P. Lin, and M. Acuña (2008), Evidence for collisionless magnetic reconnection at Mars, *Geophys. Res. Lett.*, *35*, L02106, doi:10.1029/2007GL032289.
Eastwood, J. P., J. J. H. Videira, D. A. Brain, and J. S. Halekas (2012), A chain of magnetic flux ropes in the magnetotail of Mars, *Geophys. Res. Lett.*, *39*, L03104, doi:10.1029/2011GL050444.
Elphic, R. C., and C. T. Russell (1983), Evidence for helical kink instability in the Venus magnetic flux ropes, *Geophys. Res. Lett.*, *10*, 459–462, doi:10.1029/GL010i006p00459.
Fedorov, A., et al. (2006), Structure of the Martian wake, *Icarus*, *182*, 329–336, doi:10.1016/j.icarus.2005.09.021.
Fedorov, A., et al. (2008), Comparative analysis of Venus and Mars magnetotails, *Planet. Space Sci.*, *56*, 812–817, doi:10.1016/j.pss.2007.12.012.
Halekas, J. S., and D. A. Brain (2010), Global distribution, structure, and solar wind control of low altitude current sheets at Mars, *Icarus*, *206*, 64–73, doi:10.1016/j.icarus.2008.12.032.
Halekas, J. S., J. P. Eastwood, D. A. Brain, T. D. Phan, M. Øieroset, and R. P. Lin (2009), In situ observations of reconnection Hall magnetic fields at Mars: Evidence for ion diffusion region encounters, *J. Geophys. Res.*, *114*, A11204, doi:10.1029/2009JA014544.
Halekas, J. S., et al. (2016), Plasma clouds and snowplows: Bulk plasma escape from Mars observed by MAVEN, *Geophys. Res. Lett.*, *43*, 1426–1434, doi:10.1002/2016GL067752.
Hara, T., K. Seki, H. Hasegawa, D. A. Brain, K. Matsunaga, and M. H. Saito (2014a), The spatial structure of Martian magnetic flux ropes recovered by the Grad-Shafranov reconstruction technique, *J. Geophys. Res. Space Physics*, *119*, 1262–1271, doi:10.1002/2013JA019414.
Hara, T., K. Seki, H. Hasegawa, D. A. Brain, K. Matsunaga, M. H. Saito, and D. Shiota (2014b), Formation processes of flux ropes downstream from Martian crustal magnetic fields inferred from Grad-Shafranov reconstruction, *J. Geophys. Res. Space Physics*, *119*, 7947–7962, doi:10.1002/2014JA019943.
Hara, T., et al. (2015), Estimation of the spatial structure of a detached magnetic flux rope at Mars based on simultaneous MAVEN plasma and magnetic field observations, *Geophys. Res. Lett.*, *42*, 8933–8941, doi:10.1002/2015GL065720.
Hara, T., et al. (2016), MAVEN observations of magnetic flux ropes with a strong field amplitude in the Martian magnetosheath during the ICME passage on 8 March 2015, *Geophys. Res. Lett.*, *43*, 4816–4824, doi:10.1002/2016GL068960.
Hara, T., et al. (2017), MAVEN observations of a giant ionospheric flux rope near Mars resulting from interaction between the crustal and interplanetary draped magnetic fields, *J. Geophys. Res. Space Physics*, *122*, 828–842, doi:10.1002/2016JA023347.
Harada, Y., et al. (2015a), Marsward and tailward ions in the near-Mars magnetotail: MAVEN observations, *Geophys. Res. Lett.*, *42*, 8925–8932, doi:10.1002/2015GL065005.
Harada, Y., et al. (2015b), Magnetic reconnection in the near-Mars magnetotail: MAVEN observations, *Geophys. Res. Lett.*, *42*, 8838–8845, doi:10.1002/2015GL065004.
Harada, Y., et al. (2017), Survey of magnetic reconnection signatures in the Martian magnetotail with MAVEN, *J. Geophys. Res. Space Physics*, *122*, 5114–5131, doi:10.1002/2017JA023952.
Hasegawa, H. (2012), Structure and dynamics of the magnetopause and its boundary layers, *Monogr. Environ. Earth Planets*, *1*, 71–119, doi:10.5047/meep.2012.00102.0071.
Huddleston, D. E., C. T. Russell, M. G. Kivelson, and J. G. Luhmann (1996), Time delays in the solar wind flow past Venus: Galileo-Pioneer Venus correlations, *J. Geophys. Res.*, *101*, 4539–4546, doi:10.1029/95JE02774.
Jakosky, B. M., et al. (2015), The Mars Atmosphere and Volatile EvolutioN (MAVEN) mission, *Space Sci. Rev.*, *195*, 3–48, doi:10.1007/s11214-015-0139-x.
Kollmann, P., P. C. Brandt, G. Collinson, Z. J. Rong, Y. Futaana, and T. L. Zhang (2016), Properties of planetward ion flows in Venus' magnetotail, *Icarus*, *274*, 73–82, doi:10.1016/j.icarus.2016.02.053.
Lepping, R. P., L. F. Burlaga, and J. A. Jones (1990), Magnetic field structure of interplanetary magnetic clouds at 1 AU, *J. Geophys. Res.*, *95*, 11,957–11,965, doi:10.1029/JA095iA08p11957.
Luhmann, J. G., and T. E. Cravens (1991), Magnetic fields in the ionosphere of Venus, *Space Sci. Rev.*, *55*, 201–274, doi:10.1007/BF00177138.
Luhmann, J. G., C. T. Russell, and R. C. Elphic (1984), Time scales for the decay of induced large-scale magnetic fields in the Venus ionosphere, *J. Geophys. Res.*, *89*, 362–368, doi:10.1029/JA089iA01p00362.
Lundin, R., H. Borg, B. Hultqvist, A. Zakharov, and R. Pellinen (1989), First measurements of the ionospheric plasma escape from Mars, *Nature*, *341*, 609–612, doi:10.1038/341609a0.
McFadden, J. P., et al. (2015), MAVEN SupraThermal and Thermal Ion Composition (STATIC) instrument, *Space Sci. Rev.*, *195*, 199–256, doi:10.1007/s11214-015-0175-6.
Mitchell, D. L., et al. (2016), The MAVEN Solar Wind Electron Analyzer, *Space Sci. Rev.*, *200*, 495–528, doi:10.1007/s11214-015-0232-1.
Morschhauser, A., V. Lesur, and M. Grott (2014), A spherical harmonic model of the lithospheric magnetic field of Mars, *J. Geophys. Res. Planets*, *119*, 1162–1188, doi:10.1002/2013JE004555.
Rong, Z. J., W. X. Wan, C. Shen, T. L. Zhang, A. T. Y. Lui, Y. Wang, M. W. Dunlop, Y. C. Zhang, and Q.-G. Zong (2013), Method for inferring the axis orientation of cylindrical magnetic flux rope based on single-point measurement, *J. Geophys. Res. Space Physics*, *118*, 271–283, doi:10.1029/2012JA018079.

Rong, Z. J., S. Barabash, G. Stenberg, Y. Futaana, T. L. Zhang, W. X. Wan, Y. Wei, X. D. Wang, L. H. Chai, and J. Zhong (2015), The flapping motion of the Venusian magnetotail: Venus Express observations, *J. Geophys. Res. Space Physics*, *120*, 5593–5602, doi:10.1002/2015JA021317.

Ruhunusiri, S., et al. (2016), MAVEN observations of partially developed Kelvin-Helmholtz vortices at Mars, *Geophys. Res. Lett.*, *43*, 4763–4773, doi:10.1002/2016GL068926.

Russell, C. T., and R. C. Elphic (1979), Observation of magnetic flux ropes in the Venus ionosphere, *Nature*, *279*, 616–618, doi:10.1038/279616a0.

Shimazu, H., and M. Tanaka (2008), Numerical simulation of small-scale low-β magnetic flux ropes in the upper ionospheres of Venus and Mars, *Planet. Space Sci.*, *56*, 1542–1551, doi:10.1016/j.pss.2008.07.007.

Shinagawa, H., and T. E. Cravens (1988), A one-dimensional multispecies magnetohydrodynamic model of the dayside ionosphere of Venus, *J. Geophys. Res.*, *93*, 11,263–11,277, doi:10.1029/JA093iA10p11263.

Slavin, J. A., et al. (2009), MESSENGER and Venus Express observations of the solar wind interaction with Venus, *Geophys. Res. Lett.*, *36*, L09106, doi:10.1029/2009GL037876.

Sonnerup, B. U. Ö., and M. Scheible (1998), Minimum and maximum variance analysis, in *Analysis Methods for Multi-Spacecraft Data, ISSI Sci. Rep. Ser.*, vol. 1, edited by G. Paschmann and P. W. Daly, pp. 185–220.

Vignes, D., M. H. Acuña, J. E. P. Connerney, D. H. Crider, H. Rème, and C. Mazelle (2004), Magnetic flux ropes in the Martian atmosphere: Global characteristics, *Space Sci. Rev.*, *111*, 223–231, doi:10.1023/B:SPAC.0000032716.21619.f2.

Wolff, R. S., B. E. Goldstein, and C. M. Yeates (1980), The onset and development of Kelvin-Helmholtz instability at the Venus ionopause, *J. Geophys. Res.*, *85*, 7697–7707, doi:10.1029/JA085iA13p07697.

Xiao, C. J., Z. Y. Pu, Z. W. Ma, S. Y. Fu, Z. Y. Huang, and Q. G. Zong (2004), Inferring of flux rope orientation with the minimum variance analysis technique, *J. Geophys. Res.*, *109*, A11218, doi:10.1029/2004JA010594.

Xu, S., et al. (2017), Martian low-altitude magnetic topology deduced from MAVEN/SWEA observations, *J. Geophys. Res. Space Physics*, *122*, 1831–1852, doi:10.1002/2016JA023467.

Zhang, T. L., et al. (2012), Magnetic reconnection in the near Venusian magnetotail, *Science*, *336*, 567–570, doi:10.1126/science.1217013.